Nuclear Instruments and Methods in Physics Research B 272 (2012) 74–77

Contents lists available at ScienceDirect

Nuclear Instruments and Methods in Physics Research B

journal homepage: www.elsevier.com/locate/nimb

# Ion beam studies of Ge diffusion in $Al_2O_3$

E.G. Barbagiovanni *, S.N. Dedyulin, P.J. Simpson, L.V. Goncharova

*Department of Physics and Astronomy, The University of Western Ontario, London, Ontario, Canada N6A 3K7*

ARTICLE INFO

*Article history:*
Available online 16 February 2011

*Keywords:*
Diffusion
Desorption
Nano-Crystals
Ge
$Al_2O_3$

ABSTRACT

Rutherford backscattering spectroscopy (RBS) has been used in combination with X-ray photoemission spectroscopy (XPS) to investigate Ge diffusion in $Al_2O_3$ (0001) samples. Ge was implanted in c-plane $\alpha$-$Al_2O_3$ (0001) at 80 keV to a fluence of $1 \times 10^{16}$ cm$^{-2}$ at room temperature followed by thermal annealing in the 30–180 min range at 1200 °C in a $N_2$ environment. RBS results indicate that implantation-induced damage does not fully amorphize the substrate, while incurred defects are partially annealed after 1 h accompanied by Ge phase crystallization. XPS data confirms the existence of $GeO_2$ and GeO. There is a decrease in the Ge content compared to the as-implanted sample, attributed to GeO desorption, which is evident after 30 min and by 180 min 15% of the original Ge concentration remains. Integrated intensity of the Ge peak in aligned geometry is much lower compared to random geometry with a bimodal distribution of Ge evident in both spectra indicating Ge substitutional incorporation and the formation of a distinct Ge layer. XPS data shows a peak thought to be associated with the distinct Ge layer at ≈1216.5 eV, which is a lower binding energy than a Ge reference peak. The lower binding energy is thought to result from a net positive electron density in the substrate due to excess Al atoms in the peak defect-region.



## 1. Introduction

Ge nanocrystals (ncs) are a promising material for non-volatile memory applications and integrated optoelectronics [1,2]. With a negative conduction band offset with respect to a Si substrate, faster transition rates can be achieved than in Si-ncs. However, producing efficient light-emitting Ge-ncs is a challenge. Photoluminescence from Ge-ncs in $SiO_2$ has been attributed to oxygen-related defects at the Ge-ncs/$SiO_2$ interface. When the matrix material is crystalline, optical properties of Ge-ncs may be affected by the compressive stress induced by the matrix. Ge is also more prone to form lattice defects from the stress of the surrounding matrix compared to Si [3]. The dynamics of radiative luminescence are strongly dependent on the geometry of the system; see for example [4], which motivates a detailed investigation into the mechanism(s) of Ge diffusion and nucleation during Ge-ncs growth [5,6]. Diffusion-related phenomena of Ge in $\alpha$-$Al_2O_3$ were also reported by Xu et al. [7], who observed a bimodal depth (and corresponding size) distribution of Ge-ncs using transmission electron microscopy. They further suggested that Ge has a depth dependent diffusion constant.

In this article, Ge diffusion in a crystalline $Al_2O_3$ matrix is studied using ion implantation, Rutherford backscattering spectroscopy (RBS), and X-ray photoemission spectroscopy (XPS) to deduce the elemental depth profiles and chemical environments of Ge in $Al_2O_3$, respectively. This work suggests that Ge-ncs formation is limited to a narrow range of annealing time. Further, in the case of a bimodal distribution for Ge, one Ge layer is pinned to the maximum of Ge implantation.

## 2. Experiment

Samples were prepared by $Ge^-$ ion-implantation into c-plane $\alpha - Al_2O_3$ (0001) (Valley Design Corp.) at 80 keV, 7° incidence, fluence of $1 \times 10^{16}$ cm$^{-2}$, average flux of $6.5 \times 10^9$ cm$^{-2}$ s$^{-1}$, room temperature and $10^{-7}$ Torr. The samples were then thermally processed in a tube furnace at 1200 °C in flowing $N_2$. The furnace was pumped down to ≈25 mtorr prior to annealing, to remove possible contaminants. The annealing was conducted for 30, 60, 120 and 180 min, while an as-implanted sample was not annealed as a reference.

RBS spectra were measured using incident 500 keV $^4He^+$ ions produced by a 1.7 MV Tandetron facility, with a Si charged particle detector. Typical resolution was ≈100 Å, on the surface and deteriorated with sample depth. 'Aligned' geometry spectra were obtained with the incident beam aligned in the $Al_2O_3$ [0001] channelling direction and the detector positioned at a scattering angle of 170°. 'Random' geometry spectra were acquired with the samples continuously rotated around the azimuth with a tilt angle of 3° in order to minimize channelling effects.

* Corresponding author. Tel.: +1 519 661 2111x86280.
*E-mail addresses:* ebarbagi@uwo.ca (E.G. Barbagiovanni), sdedyuli@uwo.ca (S.N. Dedyulin), psimpson@uwo.ca (P.J. Simpson), lgonchar@uwo.ca (L.V. Goncharova).

0168-583X/$ - see front matter © 2011 Elsevier B.V. All rights reserved.
doi:10.1016/j.nimb.2011.01.036

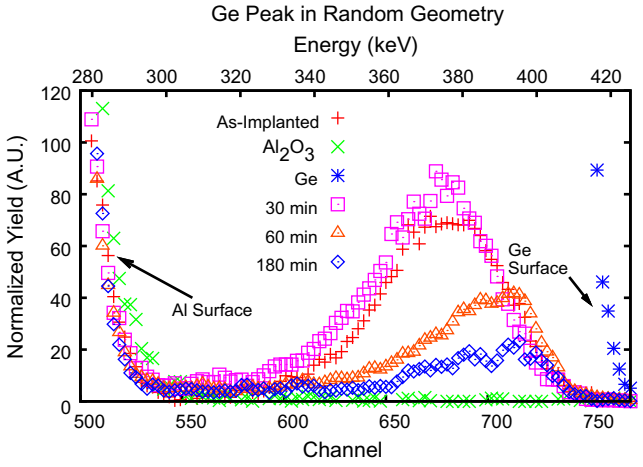


**Fig. 1.** RBS data in random geometry for the Ge peak in $Al_2O_3$ substrate as a function of annealing time. 'As-Implanted' label refers to no anneal. '$Al_2O_3$' and 'Ge' correspond to the single crystal pure $Al_2O_3$ and Ge (001) substrates. '30 min,' '60 min' and '180 min' labels refer to annealing times, '120 min' is not shown for clarity. Depth scale gives the Ge implantation depth, 0 nm is the samples surface; *scale*: 0 nm = *channel* 740 *and* 70 nm = *channel* 600. Note a split Ge peak (bimodal Ge distribution) after the 180 min anneal.

The X-ray photoemission spectroscopy (XPS) analyses were carried out with a Kratos Axis Ultra spectrometer using a monochromatic Al K(alpha) source (15 mA, 14 kV) at Surface Science Western. The instrument work function was calibrated to give a binding energy (BE) of 83.96 eV for the Au 4f7/2 line for metallic gold and the spectrometer dispersion was adjusted to give a BE of 932.62 eV for the Cu 2p3/2 line of metallic copper. High resolution analyses were carried out with an analysis area of $300 \times 700\ \mu m^2$ and a pass energy of 20 eV. Spectra were charge-corrected to C1s at 284.8 eV. In addition, due to the implantation depth of the Ge in the $Al_2O_3$ matrix, $Ar^+$ sputtering was performed at 4 kV, $4 \times 4\ mm^2$ spot, current density $39\ \mu A/cm^2$, 7 nm/min sputter rate as calibrated to an $Al_2O_3$/Al standard. Sputtering was interrupted when the Ge concentration was within the depth resolution of the XPS analysis, typically $3 \rightarrow 5$ nm, so as to avoid preferential sputtering effects.

## 3. Results and discussion

The results for RBS data in a random geometry are presented in Fig. 1. The energy scale is adjusted to highlight the Ge peak. The Al and O features are the same in all samples. Charging is a significant problem in collecting spectra from $Al_2O_3$ samples. To correct for this fact samples are aligned to the Al surface channels to monitor changes in the Ge peak, namely, Ge content and distribution with increasing annealing time. The spectrum corresponding to a 120 min anneal is not shown for clarity as it lies close to the curve for the 60 min annealed sample.

In Fig. 1, as annealing time increases, the Ge peak integrated intensity decreases. Initially a concentration of $1 \times 10^{16}\ cm^{-2}$ of Ge atoms was implanted in the sample. Simulations predict a concentration of $9.87 \times 10^{15}\ cm^{-2}$ for the as-implanted sample, in very good agreement with the experimental value. After 180 mins of annealing, the final Ge concentration is 15% of the original implantation fluence. The Ge concentrations as a function of annealing time are listed in Table 1. Fig. 1 also shows a small displacement of the Ge peak towards the surface. The displacement of the Ge peak towards the surface and the lowering of the Ge content is an indication of desorption from the sample. These effects were also observed in the work of Sharp et al. [3]. XPS data, discussed below, show the existence of GeO, which is the likely candidate for Ge desorption [8].

**Table 1**
Calculated Ge concentration as a function of annealing time. All samples were implanted to $1 \times 10^{16}$ Ge atoms.

| Sample (min) | Concentration ($\times 10^{15}\ cm^{-2}$) | Crystalline factor |
|---|---|---|
| As-Implanted | 9.87 | 0 |
| 30 | 6.68 | – |
| 60 | 3.35 | 0.55 |
| 120 | 4.17 | 0.55 |
| 180 | 1.63 | 0.5 |

In Fig. 2, Ge depth profiles obtained by calculations using SIMNRA [9] and TRIM-simulated Ge profile and vacancy concentrations are given for all annealing times.[1] TRIM calculates a maximum of Ge at a depth of ≈35 nm. Even after 30 min there exists a ≈30% decrease in the Ge concentration; albeit, very little Ge migration closer to the surface. At 60 min, the Ge profile has shifted into the defect-rich region of the sample, produced from the implantation process. This peak in the defect region, around 10 nm, does not change significantly with further annealing, while annealing does continue to produce desorption of Ge. This splitting of the Ge peak after 60 min indicates a preferential incorporation of Ge in the $Al_2O_3$ matrix (discussed further below) near the original implantation depth maximum along with preferential displacement of Ge to the defect-rich region.

A more detailed understanding of Ge phase formation in the $\alpha - Al_2O_3$ substrates is gained by looking at the aligned RBS data, shown in Fig. 3. Both the Al and the Ge energy regions are displayed. 60 min and 120 min spectra are very similar; therefore, only the curve for the 120 min sample is shown for clarity. The as-implanted sample shows partial alignment through the presence of an Al surface peak. Therefore, the $Al_2O_3$ substrate was not fully amorphized during the implantation.

This is consistent with the implantation conditions used by Budai et al., who state that if $Al_2O_3$ remains in the $\alpha$-phase during implantation any nanocrystal formation will also be in the $\alpha$-phase [10]. Angular scans (not shown here) substantiate partial amorphization of the substrate lattice since Al and O channels showed hexagonal symmetry in the channelling minima. Furthermore, a substantial number of Al atoms are displaced from their lattice positions, thus forming an Al sub-surface peak near channels 400–450, noted in Fig. 3. The sub-surface Al peak is at 35–40 nm, which is slightly deeper than the maximum Ge concentration. We can; therefore, tentatively assign this peak to the Al interstitial atoms produced during implantation. A similar subsurface peak is observed for oxygen (not shown), but it is less pronounced due to the differences in the scattering cross section. The spectrum for a 30 min anneal is not presented because it was not possible to obtain reasonable alignment with this sample. This may be due to diffusion in the Al sublattice, or partial-recrystallization of the $Al_2O_3$ substrate may be not yet completed after 30 min.

After 60–120 min, there is a strong reduction of the Al surface peak and the Ge concentration compared to the as-implanted sample. The Al surface peak becomes comparable to the one for the pure $Al_2O_3$ substrate, while the Al sub-surface peak decreases, but ion yields are still higher than pure $Al_2O_3$ substrate values. At 180 min, the Al surface peak cannot be resolved and only 15% of the as-implanted Ge concentration is remaining. Angular scans reveal channelling minima in the 180 min sample and the ion yield

[1] Vacancy profile does not correspond to the absolute defect concentration, which may be orders of magnitude less than that shown due to recombination, while the profile does indicate a ≈20 nm region of high defect concentration.

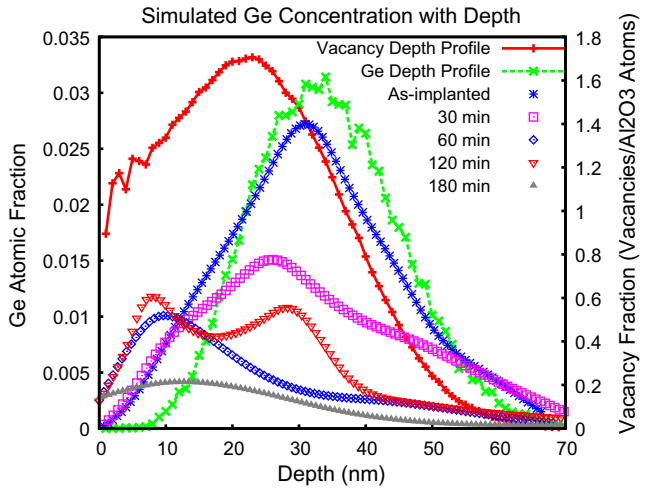


**Fig. 2.** Calculated Ge concentration in atomic fractions as a function of depth for different annealing times in a $Al_2O_3$ substrate. 'Vacancy Depth Profile' was obtained from TRIM [15]; and plotted in vacancy sights per sum of substrate atom units. 'Ge Depth Profile' is also obtained from TRIM. Due to smoothing of data and the resolution of RBS data, the simulated peak at ≈30 nm is not shown for '60 min' and '180 min'.

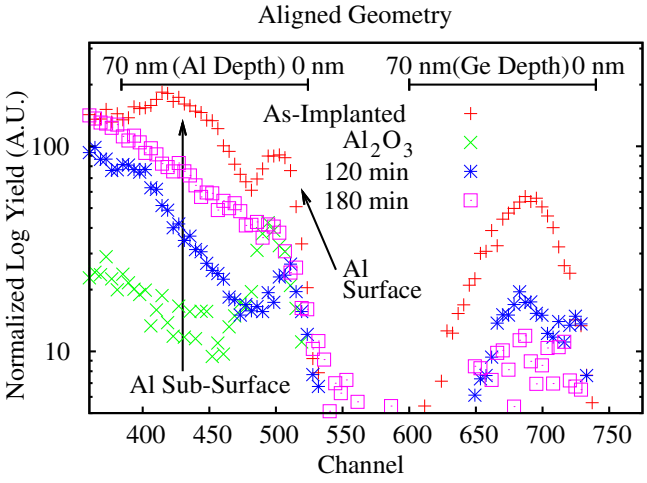


**Fig. 3.** Backscattering data (log scale) for the [0001] $Al_2O_3$ aligned geometry. 'Al Surface' indicates position of the surface Al peak. 'Al Sub-Surface' labels the Al region resulting from partial disorder of the substrate. Depth scale gives the Ge implantation depth, 0 nm is the samples surface; *scale*: 0 nm = *channel* 740 and 70 nm = *channel* 600. Note bimodal distribution of Ge peak in the 120 min annealed sample.

is higher compared with the pure $Al_2O_3$ sample. These facts indicate that the sample is still crystalline; however, the Al surface peak is not visible, which can be an indication that residual Ge has been incorporated into the $Al_2O_3$ matrix.

Using the aligned spectra in comparison to the random, one can define the degree of crystallization of the Ge phases. That is, by defining a crystallinity factor, $1-c$, where $c$ is the ratio of the aligned peak intensity, $a$, to the random peak intensity, $r$, then: $1-c=1-\frac{a}{r}$. Recalling that the 30 min sample did not align well does not allow such a determination for $c$. With the 60 min and 120 min samples being very close in peak intensity yields: $1-c_{60/120}=0.55$. For the 180 min sample: $c_{180}=0.5$, but most of the Ge is lost. There is little variation in the crystallinity of Ge with annealing time, which indicates that Ge-ncs are formed after $\geqslant$60 min of annealing. Based on the previous discussion of continued desorption of Ge as a limit in producing Ge-ncs, this result indicates that short annealing times and/or high Ge content are sufficient to produce Ge-ncs. Noting that the Ge atomic concentration never exceeds a peak value of ≈1% in the defect region, as seen in Fig. 2, further substantiates the previous assertion and the fact that only Ge desorption continues with time. Furthermore, as discussed in Sharp et al., Ge-ncs tend to align in a crystalline phase such that $(111)_{Ge}\|(\bar{1}104)_{Al_2O_3}$ [3].

XPS data were analysed using CasaXPS software (version 2.3.15) with Shirley background and Gaussian–Lorentzian line shapes [11]. As in the RBS data, charging is a significant problem. To correct for this problem spectra were corrected to the C1s peak set at 284.8 eV, which has an associated error of $\pm 0.1 \rightarrow 0.2$ eV [12]. Even with this correction, relative binding energies must be evaluated cautiously because Ar sputtering preferentially displaces O [13]. If we assume that differences in chemical environment due to preferential sputtering create variations in the O concentration near the surface region, than using the published values for $GeO_2$ 2p3/2 (1220.6 eV) versus GeO 2p3/2 (1219.3 eV), yields an associated error [14]. As mentioned in the experimental section, sputtering is carried out only to expose the initial Ge concentration.

XPS spectra for the Ge 2p3/2 are shown in Fig. 4. The 2p3/2 peak in the Ge reference sample corresponds exactly with the reported value (1217.6 eV) [14]. For all of the samples there are two peaks, which can be deconvoluted into the Ge and $GeO_x$ components (shown in the caption), The $GeO_x$ peak is at ≈1219.5 eV, exact values are given in the figure. Based on the oxide values presented above, this peak corresponds to germanium oxides. Furthermore, this peak has a FWHM of ≈2 eV. Based on the published value described above, this peak can be ascribed as a convolution of GeO and $GeO_2$. Note that as annealing temperature increases the ratio of $GeO_x$ to Ge increases as well. These $GeO_x$ can be either a phase

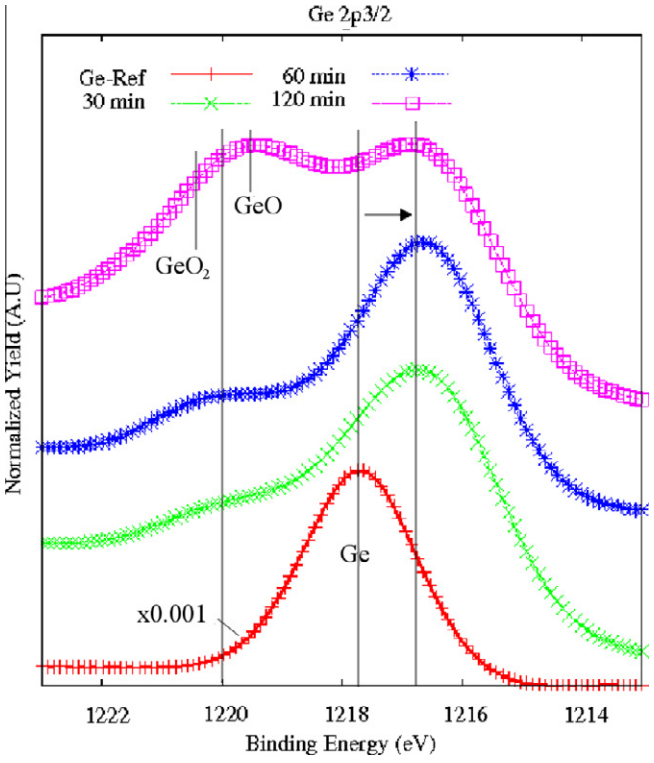


**Fig. 4.** XPS data for Ge 2p3/2 as a function of annealing time, labelled in plot. Peak position values (eV) with FWHM values (eV) in parenthesis are: Ge-ref: 1217.67 (1.13); 30 min: 1219.29 (2.72) & 1216.52 (1.91); 60 min: 1219.84 (2.02) & 1216.57 (1.63); 120 min: 1219.45 (2.24) & 1216.56 (1.72).

**Table 2**
XPS Ge 3d3/2 and 3d5/2 peak position and FWHM as a function of annealing time.

| Sample (min) | Spin-orbit | Position (eV) | FWHM (eV) |
|---|---|---|---|
| Ge-ref | 3/2: | 30.01 | 0.73 |
| | 5/2: | 29.50 | 0.73 |
| 30 | 3/2: | 32.93 | 0.86 |
| | 5/2: | 32.33 | 0.86 |
| 60 | 3/2: | 32.79 | 0.84 |
| | 5/2: | 32.19 | 0.84 |
| 120 | 3/2: | 32.30 | 1.05 |
| | 5/2: | 31.70 | 1.05 |

segregated region near, surrounding Ge-ncs, or this can be Ge in the $Al_2O_3$ matrix. The existence of GeO explains the desorption process described earlier. GeO is known to desorb from the from $GeO_2$ [8].

Fig. 4 also shows an intensity at ≈1216.5 eV for all samples. The literature does not report a peak at this energy; therefore, without further experiments a speculative existence is ascribed. With the formation of Ge oxides in the substrate and oxygen vacancies still remaining in $Al_2O_3$ sublattice, Al is left with less oxygen in the nearest neighbour coordination. Since Al has a positive electrical affinity, the local electron density will be adjusted accordingly. This fact means that Ge atoms in the vicinity of under-coordinated Al atoms (i.e. Ge–Al direct bond formation) may experience a lowering of their binding energy. Alternatively, this peak is associated with Ge-ncs in the defect-rich region. Furthermore, the possibility that this peak shift is due to stress on Ge-ncs is ruled out based on the fact that Ge-ncs are reported to experience a compressive stress of 2.5 GPa as noted by a blue shift in the Raman spectra, which would appear as a shift to a higher binding energy in XPS [3]. Finally, it is noted that the experiment was repeated several times to ensure that this peak was not an artefact of charging in the sample.

Ge 3d3/2 and 3d5/2 peak positions are presented in Table 2, with a binding energy split fixed at 0.6 eV and a branching ratio of 3:2, respectively. Note that XPS data could not be obtained for the 180 min sample, due to the low Ge concentration. Although there is an increase in the full-width half max (FWHM) for each of the samples, considering the errors of the experiment this increase cannot be associated with initial-final states effects of charging. However, it is possible that the shift to a higher binding energy in all samples is due to stress on Ge-ncs [3]. Note also that the 3p peak does not appear in any of the samples.

The experimental conditions are in accord with the formation of Ge-ncs [3], in addition, XPS data (Ge phase formation) and RBS data (crystallization in Ge phase) findings support this fact. Furthermore, according to [3] Ge-ncs form in the defect-rich region of the sample; therefore, the Ge peak in the defect region is labelled as resulting from Ge-ncs. In terms of nanocrystal formation this bimodal distribution and continued decrease in Ge concentration means that the Ge-ncs are highly sensitive to annealing conditions; thereby, they are destroyed or reduced in number with extended annealing times. Therefore, to form Ge-ncs, short annealing times and/or an annealing environment that prevents desorption of Ge must be used.

## 4. Conclusions

Ge implanted $Al_2O_3$ samples were studied across varying annealing durations at 1200 °C using RBS and XPS. RBS data indicated that peak of the Ge implant concentration begins to migrate after a 30 min anneal. After a 60 min anneal, the Ge concentration forms a bimodal distribution with a peak near the original implantation depth and a second peak in the peak defect region of the sample. This trend continues with longer annealing times; in addition, Ge desorption was observed across all samples. XPS data indicated the existence of GeO and $GeO_2$ in the samples, in a convoluted peak around 1219.5 eV. GeO is ascribed as the desorping species in the samples. Furthermore, it is believed that the oxides are formed due to displacement of the Al atoms from the substrate matrix, leading to incorporation of Ge. Aligned RBS data for the 'as-implanted' sample was composed of an 'Al sub-surface' peak, which indicated the displacement of Al atoms from their respective lattice positions. All the while, there remained, in that sample, an Al 'surface' peak indicating that the substrate was not fully amorphized during ion implantation. During annealing, there was a reduction in the Al 'surface' peak, which was removed after a 180 mins of annealing. This observation was an indication of Ge incorporation.

Ge-nc formation was discussed through the use of a crystallinity factor, defined by comparing the yield of the aligned to random RBS geometry. This factor indicated a crystallinity of ≈0.5 in all samples, indicating that Ge-nc formation occurs after ≈60 mins of annealing at this temperature; furthermore, the Ge-ncs were believed to exist in the peak defect region. While, due to continued desorption, it is concluded that increased annealing time destroys Ge-nc. XPS data also contained a peak around 1216.5 eV, which was associated with the distinct layer of Ge-ncs. To the best of our knowledge, this peak has not been reported elsewhere. It was positioned at a lower binding energy than a Ge reference peak. This fact was understood as the Ge-ncs existing in a region of positive electron density. Further work must be carried out to firmly establish the meaning of this peak.

We gratefully acknowledge Mark Biesinger at Surface Science Western for work on the XPS data and many valuable discussions; Jack Hendrix of the Western Tandetron Accelerator Facility for valuable help with ion implantation. Funding was provided from NSERC/CRSNG and the University of Western Ontario.

## References

[1] P. Dimitrakis, A. Mouti, C. Bonafos, S. Schamm, G.B. Assayag, V. Ioannou-Sougleridis, B. Schmidt, J. Becker, P. Normand, Microelectron. Eng. 86 (2009) 1838.
[2] Y.Q. Wang, J.H. Chen, W.J. Yoo, Y.C. Yeo, S.J. Kim, R. Gupta, Z.Y.L. Tan, D.L. Kwong, A.Y. Du, N. Balasubramanian, Appl. Phys. Lett. 84 (2004) 5407.
[3] I.D. Sharp, Q. Xu, D.O. Yi, C.W. Yuan, J.W. Beeman, K.M. Yu, J.W. Ager D.C. Chrzan, E.E. Haller, J. Appl. Phys. 100 (2006) 114317.
[4] A.D. Yoffe, Adv. Phys. 51 (2002) 799.
[5] K.S. Min, K.V. Shcheglov, C.M. Yang, H.A. Atwater, M.L. Brongersma, A. Polman, Appl. Phys. Lett. 69 (1996) 2033.
[6] X.L. Wu, T. Gao, G.G. Siu, S. Tong, M. Bao, Appl. Phys. Lett. 74 (1999) 2420.
[7] Q. Xu, I.D. Sharp, D.O. Yi, C.Y. Liao, D.C. Chrzan, E.E. Haller, J.W. Beeman K.M. Yu, J.W. Ager III, Am. Phys. Soc. L17 (2005) 00009. March.
[8] K. Prabhakaran, F. Maeda, Y. Watanabe, T. Ogino, Appl. Phys. Lett. 76 (2000) 2244.
[9] M. Mayer, SIMNRA user's guide. Tech.Rep.IPP9/113, Max-Plank-Institut fur Plasmaphysik, Garching, Germany, 1997.
[10] J.D. Budai, C.W. White, S.P. Withrow, M.F. Chisholm, J. Zhu, R.A. Zuhr, Nature 390 (1997) 384.
[11] CasaXPS. <http://www.casaxps.com/>,Version 2.3.15 2009.
[12] D.J. Miller, M.C. Biesinger, N.S. McIntyre, Surf. Interface Anal. 33 (2002) 299.
[13] H. Lee, S.M. Lee, E.T. Ada, B. Kim, M. Weiss, S.S. Perry, J.W. Rabalais, Nucl. Instrum. Meth. B 157 (1999) 226.
[14] K. Prabhakaran, T. Ogino, Surf. Sci. 325 (1995) 263.
[15] J.F. Ziegler, J.P. Biersack, U. Littmark, The Stopping and Range of Ions in Solids, Pergamon Press, New York, 1985.